Published in final edited form as:

J Immunol. 2016 September 1; 197(5): 1926–1936. doi:10.4049/jimmunol.1600162.

Extensive citrullination promotes immunogenicity of HSP90 through protein unfolding and exposure of cryptic epitopes[1]

Timothy S. Travers[*,2], **Lisa Harlow**[†], **Ivan O. Rosas**[‡], **Bernadette R. Gochuico**[§], **Ted R. Mikuls**[¶], **Sanjoy K. Bhattacharya**[||], **Carlos J. Camacho**[*,#], and **Dana P. Ascherman**[†,#]

[*]Department of Computational and Systems Biology, University of Pittsburgh School of Medicine, Pittsburgh, Pennsylvania 15213

[†]Department of Medicine, Division of Rheumatology, University of Miami Miller School of Medicine, Miami, Florida 33136

[‡]Department of Medicine, Division of Pulmonary and Critical Care Medicine, Brigham and Women's Hospital, Boston, Massachusetts 02115

[§]Medical Genetics Branch, NHGR, NIH, Bethesda, Maryland 20892

[¶]Department of Medicine, Division of Rheumatology, University of Nebraska Medical Center, Omaha, Nebraska 68198

[||]Department of Ophthalmology, University of Miami Miller School of Medicine, Miami, Florida 33136

Abstract

Post-translational protein modifications such as citrullination have been linked to the breach of immune tolerance and clinical autoimmunity. Previous studies from our laboratory support this concept, demonstrating that autoantibodies targeting citrullinated isoforms of HSP90 are associated with rheumatoid arthritis complicated by interstitial lung disease. To further explore the relationship between citrullination and structural determinants of HSP90 immunogenicity, we employed a combination of ELISA-based epitope profiling, computational modeling, and mass spectrometric sequencing of peptidylarginine deiminase (PAD)-modified protein. Remarkably, ELISAs involving selected citrullinated HSP90β/α peptides identified a key epitope corresponding to an internal Arg residue (R502 (HSP90β)/R510 (HSP90α)) that is normally buried within the crystal structure of native/unmodified HSP90. *In vitro* time/dose response experiments reveal an ordered pattern of PAD-mediated deimination events culminating in citrullination of R502/R510. Conventional as well as scaled molecular dynamics (MD) simulations further demonstrate that

[1]The work encompassed by this manuscript was supported by the following grants: VA Merit Review 1I01BX000788 (DPA), ACR/REF Within Our Reach Foundation Investigator Award (DPA), NIH R01 GM97082 (CJC), and Commonwealth of Pennsylvania Department of Health grant SAP 4100062224 (CJC). This work was also supported in part by the Intramural Research Program of the National Human Genome Research Institute, National Institutes of Health (BRG).

[#]Co-corresponding authors: Carlos J. Camacho, Ph.D., Department of Computational and Systems Biology, University of Pittsburgh School of Medicine, Suite 3064, Biomedical Science Tower 3, 3501 5th Avenue, Pittsburgh, Pennsylvania 15260, Phone: (412) 648-3333, FAX: (412) 648-3163, CCamacho@pitt.edu. Dana P. Ascherman, M.D., Department of Medicine, Division of Rheumatology, University of Miami Miller School of Medicine, RMSB, 7152, 1600 NW 10th Avenue, Miami, Florida 33136, Phone: (305) 243-8567, FAX: (305) 243-7414, DAscherman@med.miami.edu.

[2]Current address: Theoretical Biology and Biophysics Group, Los Alamos National Laboratory, Los Alamos, New Mexico 87545

citrullination of selected Arg residues leads to progressive disruption of HSP90 tertiary structure, promoting exposure of R502/R510 to PAD modification and subsequent autoantibody binding. Consistent with this process, ELISAs incorporating variably deiminated HSP90 as substrate antigen indicate a direct relationship between the degree of citrullination and the level of *ex vivo* antibody recognition. Overall, these data support a novel structural paradigm whereby citrullination-induced shifts in protein structure generate cryptic epitopes capable of bypassing B cell tolerance in the appropriate genetic context.

INTRODUCTION

Development of autoimmune disease reflects the breakdown of immune tolerance to self-antigens (1, 2). Although multiple mechanisms likely contribute to this process, post-translational protein modifications and the generation of “cryptic” epitopes that are seen as foreign by the host immune system play a central role in the breach of B/T cell tolerance (3–6). Particularly for B cell recognition, however, this paradigm fails to provide a complete explanation for the exposure of three dimensional conformational epitopes that are sterically obscured in the native state of complex, folded proteins. From a structural point of view, defining the relationship between post-translational modifications, protein unfolding, and accessibility to antibody binding is therefore critical for understanding factors contributing to immunogenicity of autoantigens targeted by aberrant humoral immune responses in human disease.

Among the most common systemic autoimmune diseases linked to post-translationally modified autoantigens, rheumatoid arthritis (RA) is characterized by chronic synovitis (7) as well as extra-articular manifestations that significantly contribute to morbidity and mortality (8–14). In fact, current evidence indicates that RA patients fall into distinct subsets based on the presence or absence of anti-citrullinated protein antibodies (ACPAs) (15) that generally portend a more aggressive disease course (16–18). In RA patients possessing ACPAs (approximately 70–80% (19, 20)), the autoimmune response is shaped by immune recognition of citrullinated (deiminated) autoantigens in an appropriate genetic background; for instance, the HLA-DRB1 shared epitope alleles are associated with RA primarily in the ACPA-positive subset (21–23). For these patients, a gene-environment interaction has been identified that involves an association between HLA-DRB1 alleles and injurious lung stimuli such as cigarette smoke or silica dust (24–26). Interestingly, smoking also enhances the expression of the enzyme peptidylarginine deiminase 2 (PAD2), potentially triggering increased protein citrullination in lung epithelial tissue (27). The lung therefore represents a site of putative immunologic “danger,” with induction of citrullination and breakdown of tolerance hinging on genetic susceptibility to environmental insults (28).

Based on this conceptual framework, Harlow et al. developed a “reverse immunophenotyping” approach using patient sera to define autoantibody targets in RA-associated interstitial lung disease (RA-ILD)--and identified citrullinated isoforms of heat shock protein 90 (citHSP90α, citHSP90β) as potential autoantigens (29). Comprehensive antibody profiling through ELISA-based screening demonstrated that anti-citrullinated HSP90 antibodies identified RA-ILD sera with modest sensitivity (~30%), but great

specificity (>95%). More importantly, comparative antibody assessment in sera and bronchoalveolar lavage fluid (BALF) (30) revealed both quantitative and qualitative differences in anti-citrullinated HSP90 protein/peptide profiles between matched sera and BALF specimens, providing compelling evidence that the lung is actively involved in initiating and/or shaping the humoral immune response against autoantigens such as citrullinated HSP90.

Collectively, these observations linking anti-citrullinated HSP90 antibody responses to RA-ILD led us to explore the relationship between citrulline-induced changes in protein structure and the resulting epitope specificity of targeted autoantibodies. Although a single citrullination event that replaces an arginine side chain NH_2 group with an oxygen atom is not expected to significantly impact overall protein structure, studies involving trichohyalin (31), filaggrin (31), and myelin basic protein (32) have shown that multiple modifications can promote unfolding of protein secondary and tertiary structure—with the potential to expose highly immunogenic/cryptic internal epitopes.

Because citrullinated versions of proteins such as filaggrin and myelin basic protein have, in fact, been identified as targets of RA autoantibodies (33, 34), we sought to explain how different regions of alternative autoantigens such as HSP90 become exposed to PAD enzymes and subsequent humoral immune responses. Using molecular dynamics (MD) simulations, we assessed the impact of multiple citrullination events on the tertiary structure of the HSP90 middle domain (comprising residues 303–706) that encompasses major peptide epitopes recognized by RA-ILD sera. In concert with mass spectrometry (MS) profiling of *in vitro* deiminated HSP90, these structural modeling efforts demonstrated that initial citrullination of multiple sites (i.e., hypercitrullination) is critical for inducing partial unfolding of HSP90 structure and revealing cryptic/hidden epitopes that stimulate significant autoantibody production in RA-ILD. Bolstered by ELISA-based epitope mapping studies that reflect immune responses to *in vivo* citrullination events, these observations support a structural/mechanistic paradigm linking extensive post-translational modifications to alteration of protein structure, exposure of critical immunogenic regions, and the breakdown of B cell tolerance.

METHODS

Inclusion criteria and patient samples

In accordance with approved Institutional Review Board protocols, all serum samples were obtained from previously established registries that incorporate cohorts of patients meeting the American College of Rheumatology classification criteria for RA (35). These registries included the Veterans Administration Rheumatoid Arthritis (VARA) database (36), Brigham and Women's Hospital, the National Institutes of Health (37), and the University of Pittsburgh Connective Tissue Database.

Time- and dose-dependent protein citrullination

Citrullination of recombinant HSP90β protein (Sigma-Aldrich, St. Louis, MO) was performed through *in vitro* enzymatic reactions involving incubation of recombinant HSP90

(100 μg/ml; Sigma-Aldrich, St. Louis, MO) with either high (5 units/mL) or low (0.5 units/mL) concentrations of rabbit skeletal muscle peptidylarginine deiminase (PAD; Sigma-Aldrich, St. Louis, MO) in a buffer containing 20 mM Tris (pH 8.8), 0.3 M NaCl, 1 mM EDTA, 10 mM DTT, and 5 mM $CaCl_2$. Aliquots from both *in vitro* reactions were obtained after 30, 60, 120, and 360 minutes, as well as after overnight incubation.

Mass spectrometric identification of citrullination sites

Citrullinated HSP90β protein obtained from different time points during *in vitro* citrullination reactions was digested with chymotrypsin (0.1μg/μg protein), eluted, and subjected to mass spectrometry for sequence analysis of derivative peptides on a Q-exactive Orbitrap mass spectrometer equipped with an Easy nLC 1000 nanoliquid chromatography system (Ophthalmology Mass Spectrometry Core Facility, Bascom Palmer Eye Institute, University of Miami Miller School of Medicine). Chymotrypsin-digested peptides from approximately 1 μg of HSP90 protein were loaded onto the Easy nLC 1000 using a 20-μL loop, with a flow rate of 300 nL/min and a pre-set elution gradient comprised of varying percentages of solvent A (water + 0.1% formic acid) and solvent B (acetonitrile + 0.1% formic acid) (0 to 5 minutes, 5% solvent B at 350 nL/min; 5 to 15 minutes, 5–30% solvent B at 350 nL/min; 15 to 20 minutes, 30–70% solvent B at 350 nL/min; 20 to 30 minutes, 95% solvent B at 350 nL/min). Mass spectrometry was then performed using a Q Exactive mass spectrometer (ThermoFisher Scientific). Subsequent analysis was carried out in Proteome Discoverer (Thermofisher Scientific), with minimum and maximum precursor mass settings of 350 Da and 5000 Da, respectively. Aiding the process of peptide sequencing and identification of citrulline residues, Mascot and SequestHT (UniProt) database search engines were employed with the following key parameters to generate probability scores: peptide minimal length of 6 and maximum length of 144 amino acids, fragment mass tolerance of 0.6 Da. Dynamic modifications were set to target citrullination +0.984 Da (R), and the percolator was fixed to a maximum Delta Cn of 0.05, with strict confidence of 99% and relaxed confidence of 95%.

HSP90-derived peptides

Ten 25-mer peptide sequences from HSP90β and HSP90α were derived from a previous mass spectrometric analysis of citrullinated proteins immunoprecipitated by RA-ILD patient sera (29). The ten HSP90-derived peptide sequences (9 from HSP90β, one from HSP90α) are shown in Table I. For peptides 7 and 10 (from HSP90β and HSP90α, respectively), F499 (HSP90β) and F507 (HSP90α) to alanine mutations were incorporated to generate the following peptides used as substrate antigens in ELISA (citrullination sites are shown as capitalized residues between dashes; mutated residues are also capitalized):

skeqvansaAve-R-vrkrgLevvymt (HSP90β) — 7/17-M3

tkdqvansaAve-R-lrkhgleviymi (HSP90α) — 10/20-M3

ELISA

Serum levels of IgG antibodies recognizing the HSP90-derived peptides were measured using standard solid-phase ELISA according to the following protocol that uses biotinylated peptide substrate antigens (CPC Scientific, Inc., Sunnyvale, CA) and streptavidin-coated

microplates (R&D Systems, Inc., Minneapolis, MN). ELISA plates were initially coated with either peptide pools (consisting of five peptides, each at 0.2 μg/mL) or individual peptides (1.0 μg/mL) in carbonate buffer (100 mM $NaHCO_3/Na_2CO_3$, pH 9.6) for 30 minutes. Following multiple washes with PBS/0.1% Tween-20, substrate-bound microplates were blocked for 1 hour with PBS/Tween containing 4% whey protein and 15% goat serum. Diluted serum samples (1:250) were then added for 1 hour (in competition ELISAs, diluted serum samples were pre-incubated with designated peptides/proteins for 45 minutes before being added to wells containing substrate antigen). Sequential incubations with horseradish peroxidase-conjugated, anti-human IgG secondary antibodies (0.04 mg/mL; Santa Cruz Biotechnology, Santa Cruz, CA) and 3,3,5,5-tetramethylbenzidine (TMB) (Sigma-Aldrich, St. Louis, MO) substrate permitted spectrophotometric measurements of optical density at 450 nm (OD_{450}). Ranges of relative reactivity were established for corrected OD_{450} values (OD_{450} peptide- OD_{450} no antigen control) using designated control samples for inter-assay standardization; simultaneous measurement of serum reactivity against individual peptides further facilitated intra-assay comparisons. ELISA-based assessment of antibody binding to uncitrullinated versus citrullinated HSP90 (1 μg/ml) adhered to a similar protocol employing conventional, rather than streptavidin-coated, ELISA plates (Nunc, Rochester, NY).

Homology modeling of HSP90β protein structure

We used a crystal structure for the middle domain of human HSP90α, from PDB ID 3Q6M (38), as the basis for building a homology model structure for the middle domain of human HSP90β (comprising residues 303 to 706). The middle domains for both HSP90 isoforms share 87% sequence identity and 95% sequence similarity, based on a pairwise sequence alignment performed using the EMBL-EBI web interface for EMBOSS Stretcher (39) with default parameters. *In silico* point mutations were established using PyMOL (40) to match the human HSP90β sequence.

Conventional and scaled MD simulations

All MD simulations were performed in explicit solvent using the GPU (graphics processing unit)–accelerated pmemd.cuda program from Amber version 14 (41, 42) with the Amber ff14SB force field (43). To derive AMBER-compatible parameters for citrulline, we used an approach outlined in reference (44) that derived GROMOS-compatible parameters by using GLN parameters for the side chain $CONH_2$ moiety and ARG parameters for the rest of the citrulline atoms. To prepare the HSP90β middle domain simulations, the N- and C-termini of the human HSP90β homology model structure were neutralized using acetamide and N-methylamide patches, respectively. For the HSP90-derived peptide simulations, the starting structures of the 25-mers (with unpatched termini) were taken from the homology model. All protein and peptide starting structures were then solvated with TIP3P water molecules (45) in an octahedral box, and counter ions were added to neutralize the system charge. A cutoff of 8.0 Å was used for calculating the short-range Lennard-Jones and electrostatic interactions, while long-range electrostatic contributions were computed using the particle mesh Ewald approach (46). An Amber implementation of the hydrogen mass repartitioning scheme (47) was used that allows the time step to be increased to 4 fs. All bond lengths involving hydrogen were kept constant using SHAKE (or SETTLE for water) (48, 49). Energy minimization was then performed using steepest descent for 1000 steps and then

conjugate gradient minimization for 1000 steps, with position restraints on all protein heavy atoms. This was followed by temperature equilibration at 300 K for 50 ps under canonical (NVT) ensemble conditions and then pressure equilibration at 1 atm and 300 K for another 50 ps under isothermal-isobaric (NPT) ensemble conditions, with the same position restraints. These position restraints were removed for the succeeding steps. For the conventional MDs, we performed further equilibration for 100 ns and then a production run for 1000 ns, all under NVT ensemble conditions at 300 K. For the scaled MDs, we performed the same equilibration and production runs but with the empirical scaling factor (λ) that enables enhanced sampling along the potential energy surface set to 0.65 (within the λ range of 0.5–0.7 used for typical biomolecular simulations, as outlined in reference (50)).

Analysis of MD trajectories

Visual Molecular Dynamics (VMD) (51) was used for trajectory visualization, for clustering of side chains in the peptide simulations, and for computing side chain relative solvent-exposed surface area (SASA) for the conventional and scaled MDs of the HSP90β middle domain. Moving averages at every nanosecond were computed and plotted for the relative SASA. The CPPTRAJ program (52) included with Amber was used for computing backbone RMSD and distances between atoms.

RESULTS

Mass spectrometric profiling reveals in vitro PAD-mediated hypercitrullination of HSP90

A previous mass spectrometric analysis of human HSP90 isoforms immunoprecipitated by RA-ILD sera following *in vitro* citrullination of K562 cell extracts with PAD indicated that 9 out of the 32 arginine residues in HSP90β become modified to citrulline (29) (shown with their surrounding sequences in Figure 1A and Table I, respectively). Based on the crystal structure of the closely-related HSP90α isoform (PDB ID 3Q6M (38)), we constructed a homology model for HSP90β (Figure 1B) and found that: (i) not all of these 9 citrullination sites were readily accessible to interact with a PAD molecule (particularly R502 (peptide 7 in Table I) that is buried within the protein structure (Figure 1C)) and (ii) several accessible arginines exposed on the protein surface were not found to be citrullinated (such as R337 that is adjacent to the site at R338 (peptide 4 in Table I)). These observations led us to examine factors beyond accessibility to PAD that determine how specific arginine residues become citrullinated and then targeted by humoral immune responses in RA-ILD.

To ascertain whether a requisite set of citrullination events is needed to induce structural transitions that can expose other citrullination sites as well as cryptic epitopes, we performed a time and dose response experiment involving *in vitro* citrullination of recombinant HSP90β. Detailed mass spectrometric analysis of PAD-modified HSP90β then permitted identification of citrullinated residues at different time points and different enzyme concentrations. As shown in Tables II and III (high (5 units/ml) and low (0.5 units/ml) PAD concentrations, respectively), these experiments demonstrated that more arginines of recombinant HSP90β became citrullinated compared to the original analysis of immunoprecipitated cell extract—clearly indicating that citrullination of HSP90β proceeds in a dose- and time-dependent manner, with citrullination “hot spots” that are modified at

almost all time points. These sites include the previously identified residues R82, R392, and R612 (peptides 2, 5, and 8; Table I), as well as novel sites encompassing R177, R604, R679, and R682. The site at R502, which is buried in the native protein structure (Figure 1C), gets citrullinated only at later time points, suggesting that hypercitrullination at the aforementioned "hot spots" triggers structural changes which then render R502 accessible to PAD.

Degree of citrullination does not correlate with reactivity to sera from RA-ILD patients

We next performed ELISA-based screening of sera from RA patients with various stages of ILD (using substrate peptides shown in Table I) to assess potential correlations between the extent of citrullination (based on the earlier mass spectrometric analysis) and the degree of *in vivo* antigenicity for particular sites. Peptides bound strongly by patient sera tended to demonstrate skewed profiles, with predominant recognition occurring for the citrullinated form of these peptides (Table IV). In particular, we found this pattern of recognition for peptides 3C, 4C, 6C, 7C (derived from HSP90β), and 10C (derived from HSP90α, homologous to HSP90β peptide 7C), with peptides 6C, 7C, and 10C demonstrating the highest affinity for disease-associated autoantibodies.

More detailed analysis of these peptide recognition patterns indicated that citrullination itself does not automatically confer *in vivo* immunogenicity. Among the three sites previously identified as citrullination "hot spots", for example, R/C82 (peptides 2/2C) showed no reactivity with patient sera, R/C612 (peptides 8/8C) showed only weak reactivity without clear distinction between citrullinated/uncitrullinated forms, and R/C392 showed considerable reactivity favoring (but not exclusive to) the citrullinated version of its corresponding peptide (peptide 5C). Notably, however, citrullinated forms of R502 (HSP90β, peptide 7C) and R510 (HSP90α, peptide 10C) were strongly recognized by several patient sera, despite the fact that HSP90β R502 (and presumably HSP90α R510) was citrullinated only at later time points in the previously described *in vitro* time/dose response experiments.

Citrullination does not impact the secondary structure of strongly-immunoreactive peptides

As indicated above (Table IV), ELISA-based screening of HSP90-derived peptides showed that citrullinated forms of R475 (peptide 6C) and R502 (peptide 7C) in HSP90β and R510 (peptide 10C) of HSP90α elicited the strongest antibody recognition by RA-ILD patient sera--suggesting that epitopes containing these citrullinated residues are, in fact, generated *in vivo*. Because citrullination sites in these peptides are located within helical structural elements (Figures 2A–C, top row), we assessed the impact of citrullination on the stability of secondary structures within these peptides. Using 1-μs explicit-solvent molecular dynamics (MD) simulations of these three peptides in the presence/absence of arginine-citrulline conversions, we found that the secondary structure of these peptides was preserved in both native and citrullinated states (Figures 2A–C, bottom row). Collectively, these MD simulations therefore indicated that increased antibody binding of selected citrullinated peptides relative to their uncitrullinated versions is critically dependent on specific

recognition of citrulline residues rather than secondary structural alterations of targeted epitopes.

The epitope for peptides 7/10 includes a conserved phenylalanine that undergoes citrullination-induced conformational shift

Unlike HSP90β R475, the homologous HSP90β R502 and HSP90α R510 residues strongly recognized by patient sera (in their citrullinated form) are largely buried within their respective tertiary protein structures--suggesting that these sites constitute cryptic epitopes which require significant unfolding of surrounding protein structure prior to PAD-mediated citrullination. Coupled with mass spectrometric profiling of *in vitro* time/dose response experiments, these considerations raised the question whether citrullination at single or multiple sites might be required to induce structural modifications of HSP90β/α that, in turn, could promote accessibility of HSP90β R502 (or the HSP90α R510 homologue) to PAD and subsequent antibody binding of citrullinated epitopes.

Before addressing the relationship between citrullination of distant sites and exposure of the R502/R510 residues, however, we investigated how more proximal citrullination events might impact the conformation of other amino acids (and their side chains) contributing to epitope recognition in the homologous peptides 7C and 10C. Clustering analysis based on MD simulations showed that the sampled side chain orientations of a conserved phenylalanine (F499 in HSP90β, F507 in HSP90α) underwent a shift upon deimination of R502/R510, moving from a more “inward” (Figure 3A) to a more “outward” configuration (Figure 3B). This observation suggested that F499/F507 comprise important parts of the targeted HSP90β/HSP90α epitopes, a conclusion supported by ELISAs demonstrating that peptides containing phenylalanine-alanine mutations at these sites abolished recognition by patient sera (Table V). MD simulations of these mutant peptides also revealed stable secondary structure either with or without citrullination (Figure 3C), indicating that the observed decrease in sera reactivity stemmed from loss of the phenylalanine side chain rather than destabilization of secondary structure.

Hypercitrullination destabilizes protein tertiary structure to reveal the R502/F499 epitope

Consistent with previously cited data demonstrating that both R502 and F499 in HSP90β (as well as R510 and F507 in HSP90α) are buried within the overall protein structure (Figure 1C), 1-μs MD simulations of the native (uncitrullinated) protein showed that both of these residues have low relative solvent-accessible surface area (SASA) throughout the course of modeled trajectories (Figure 4A). However, based on our mass spectrometry data and the observation that hypercitrullination of proteins such as filaggrin (31), trichohyalin (31), and myelin basic protein (32) causes structural destabilization, we surmised that extensive deimination could similarly alter the tertiary structure of HSP90β, allowing exposure of the concealed epitope containing R502 and F499 without disruption of the secondary helical structure contributing to autoantibody recognition.

To test this hypothesis, we used an approach called *scaled* MD (50) that enhances the sampling of conformations during the simulation by a simple modification of the potential energy surface of the protein. When we simulated the uncitrullinated version of HSP90β

using scaled MD, we found that R502 and F499 again remained buried throughout most of the run, despite the fact that their relative SASA showed more variability than in conventional MD simulations (Figure 4B; compare with Figure 4A). Alternatively, scaled MD simulations incorporating mass spectrometrically-demonstrated citrullination "hot spots" at R392, R604, R612, and R679 (Tables II–III) showed that deimination of these four arginine residues generated greater than 50% relative SASA for R502 and F499, most notably in the last 200 ns (Figure 4C). Additional citrullination of R475 and R682 (which showed moderate levels of citrullination by mass spectrometry) to produce a total of six citrullination sites yielded scaled MD simulations demonstrating even more conformations with both R502 and F499 having at least 50% relative SASA (Figure 4D). Experimental assessment of these MD simulations through competition ELISAs (Supplementary Table I) demonstrated that pre-incubation of patient sera with peptide 7C (containing C502) diminishes subsequent binding of fully citrullinated HSP90β, indicating that the R502/F499 epitope does become exposed with hypercitrullination and that the secondary structure/ conformation of peptide containing C502 is largely preserved in the context of the overall citrullinated protein.

In the scaled MD simulations based on citrullination of either four or six arginines, we also found that two residues near R502 in the native protein structure--V585 and D631 (see Figure 1C)--showed an increase in their alpha-carbon distance from this site (Figure 5), providing additional evidence of citrullination-induced modification of HSP90β tertiary structure. Although corresponding scaled MD runs showed an increase in alpha-carbon distances for the uncitrullinated protein as well, these changes were of lesser magnitude and occurred much later in the trajectory (compared to the scaled MD runs for citrullinated HSP90β). Most importantly, because scaled MD simulations showed that hypercitrullination did not significantly disrupt the helical motif incorporating R502 and F499 (Figure 6; RMSD ~ 1Å) despite destabilization of surrounding tertiary structure (Figure 5), these results substantiated our earlier observations with conventional MD simulations as well as the underlying hypothesis that hypercitrullination of HSP90β can expose a highly immunogenic, cryptic epitope containing R502 and F499. Further supporting this paradigm, ELISA experiments involving HSP90β deiminated for varying time periods demonstrate that antibody recognition of this autoantigen increases with progressive citrullination, mirroring the exposure and enzymatic modification of the R502/F499 epitope (Table VI).

DISCUSSION

Through mass spectrometric analysis of *in vitro*-citrullinated HSP90β, we have demonstrated that this RA-ILD-associated autoantigen undergoes time- and dose-dependent hypercitrullination at multiple arginine residues. Although several of these arginines represent citrullination "hot spots" that are modified at almost all time points, our data indicate that citrullination alone does not guarantee immunogenicity. Supporting this concept, citrullination of "hot spot" residues such as R82 and R612 yielded little or no immunoreactivity with sera derived from patients with RA/RA-ILD. Conversely, R502--a HSP90β site that is normally buried and relatively inaccessible to enzymatic modification--is highly immunogenic in its citrullinated form, with avid binding to RA-derived autoantibodies. As demonstrated by various MD simulation approaches, hypercitrullination

of HSP90β destabilizes its tertiary structure without disturbing critical secondary structural motifs—effectively exposing the region around R502 to further PAD-mediated citrullination that is responsible for generation of an important B cell epitope preferentially linked to RA-ILD (Table IV, peptide 7). Additional ELISA experiments incorporating sera derived from patients with this autoimmune disorder (Table VI, Supplementary Table I) provide compelling evidence that the extent of HSP90 citrullination has a direct impact on antibody recognition of this autoantigen, which is driven in part by exposure of R/C502 in the context of whole protein.

To better assess the structural consequences of HSP90β hypercitrullination, we supplemented conventional MD simulations with a computational, scaled MD approach (50) that enhances the sampling of conformations adopted by proteins during the course of the MD trajectory. This more detailed sampling is achieved by modifying the potential energy surface (PES) via multiplication with an empirical scaling parameter λ that ranges between 0 and 1. Decreasing the value of λ promotes flattening of the PES and lowering of barrier heights for transitions between stable or semi-stable states at PES minima locations. However, care must be taken in choosing the value of this empirical parameter λ; using a very small λ value, for instance, will essentially visit all configurations as a random walk along the PES, biasing the distribution of sampled states that will not correspond to the desired thermodynamic ensemble. For our analysis, we selected the optimal λ value by comparing tertiary structural stability of uncitrullinated HSP90β for several scaled MD runs (each with a different λ value) to that of the conventional MD run (e.g., see the relative SASA plots for R502 and F499 in Figure 3C). Based on these constraints, a λ value of 0.65 defined the lower limit of this parameter needed to stably maintain the structure of uncitrullinated HSP90β during the scaled MD trajectory, as values below 0.65 led to unfolding of uncitrullinated HSP90β. Applying the same value of λ (0.65) in the scaled MD runs of various citrullinated forms of this protein then enabled us to assess the impact of multiple citrullination events on the underlying structure of HSP90β--with the goal of determining whether hypercitrullination could modify tertiary conformation and enhance the formation of cryptic epitopes.

Although multiple arginines became citrullinated over time following *in vitro* incubation of HSP90β with PAD (Tables II and III), computer modeling (via MD simulations) of all possible combinations was not feasible. However, because four arginines (R392, R604, R612, and R679) were consistently citrullinated at all time points following incubation of HSP90β with high PAD concentrations (Table II), we used this combination of arginine residues as the “minimum” citrullination set. We intentionally excluded R82 and R177 from this analysis given the lack of known structural data regarding the connection between N-terminal and middle domains, focusing instead on the portion of HSP90β encompassing amino acids 303 to 706. For the six-citrulline simulations, we did include R682 and R475, as both of these arginines showed the next highest degree of citrullination (after R392, R604, R612, and R679) at designated time points in the high PAD concentration data set. As shown in Figures 4–6, this constellation of citrullinated residues effectively destabilizes the tertiary structure of HSP90β without disrupting critical secondary structural motifs contributing to epitope recognition in RA-ILD.

In our overall analysis, we observed that citrullination of two arginines, R55 and R338 (encompassed by peptides 1 and 4; Table I), was only detected in the original mass spectrometric characterization of whole cell extracts immunoprecipitated by RA-ILD sera. Given that subsequent assessments identifying additional/alternative citrullination sites focused on *in vitro*-modification of recombinant HSP90β, it is likely that the presence of other proteins in whole cell extracts impacted the activity of PAD or accessibility of target sites. Beyond this issue, we observed that for some sites (such as R475), citrullination occurred at early and late, but not interim, time points. These gaps likely reflect stochastic effects arising during aliquot collection for time point analysis of sites having less extensive citrullination than sites without observed gaps. Indeed, a semi-quantitative measure of overall citrullination derived from the mass spectrometric data supports this notion, demonstrating a direct correlation between degree of citrullination and consistency of detection at different time points (data not shown).

Ultimately, despite these methodological considerations and the contrived conditions of *in vitro* citrullination, this collective analysis clearly indicates that progressive citrullination of HSP90 is a relatively ordered, time- and dose-dependent process in which R502 only becomes citrullinated in the setting of extensive citrullination of non-contiguous arginine residues. In fact, recognition of internal/non-exposed citrulline residues (occurring at sites such as R502/R510) by sera derived from RA patients suggests that this sequence of progressive citrullination occurs *in vivo* (primarily because autoantibody repertoires reflect immune responses to *in vivo* structural modifications of target antigens)—fully supporting the biological plausibility of our proposed framework for the permissive role of hypercitrullination in cryptic epitope generation. Moreover, although the temporal relationship between duration of RA-ILD and degree of *in vivo* HSP90 citrullination is difficult to gauge, the development of antibody responses targeting C502 does appear to correlate with *severity* of pulmonary disease (occurring in 5/9 patients with fibrotic lung disease versus 4/35 patients with milder interstitial abnormalities in an independent cohort of RA-ILD patients (p=0.01), data not shown) and, presumably, the extent of PAD activation.

Review of the literature indicates that citrullination is an essential post-translational modification (PTM) in several biological activities (53) that include skin keratinization, myelin formation in the central nervous system (CNS), histone-mediated epigenetic regulation, and generation of neutrophil extracellular traps (NETs) needed to kill bacteria during infection (54, 55). Importantly, however, the immune system must be able to tolerate a certain degree of host protein citrullination in order to accommodate these homeostatic processes without initiating deleterious autoimmune responses. As suggested by our findings, hypercitrullination may breach this immunologic threshold and trigger autoimmunity via structural changes that expose previously hidden/cryptic epitopes.

Based on existing data showing that known RA autoantigens such as citrullinated filaggrin and citrullinated myelin basic protein (MBP) (33, 34) also undergo significant structural changes mediated by citrullination of multiple arginine residues (31, 32), this mechanism for breaching immune tolerance likely extends beyond HSP90β. In fact, serum immunoglobulin binding protein (BiP, also known as HSPA5, GRP-78, and HSP70 protein 5) represents

another autoantigen containing multiple sites of potential citrullination, only a subset of which are recognized by RA patient sera (56). Of note, one of the key epitopes encompasses R289, a citrullinated target residue that is not accessible to PAD (or autoantibodies) in the native protein conformation (Figure 7). Conversely, two nearby arginines (R279 and R283) that are surface exposed (and therefore readily susceptible to PAD-mediated citrullination) do not trigger a humoral immune response—raising the possibility that hypercitrullination of non-immunogenic portions of BiP (such as R279 and R283) can destabilize the structure of this protein so that R289 becomes accessible to PAD in the process of cryptic epitope formation. Coupled with our computational and experimental analysis of HSP90β-targeted immune responses in RA-ILD, these observations support a more general paradigm in which post-translational protein modifications such as (hyper) citrullination induce major structural alterations capable of challenging the host immune system and inducing autoimmunity.

Supplementary Material

Refer to Web version on PubMed Central for supplementary material.

Acknowledgments

The authors take full responsibility for the contents of this paper, which do not represent the views of the Department of Veterans Affairs or the United States Government.

Abbreviations

RA	rheumatoid arthritis
RA-ILD	rheumatoid arthritis-associated interstitial lung disease
PAD	peptidylarginine deiminase
HSP90	heat shock protein 90
MD simulation	molecular dynamics simulation

References

1. Goodnow CC, Sprent J, Fazekas de St Groth B, Vinuesa CG. Cellular and genetic mechanisms of self tolerance and autoimmunity. Nature. 2005; 435:590–597. [PubMed: 15931211]
2. Pillai S. Rethinking mechanisms of autoimmune pathogenesis. J Autoimmun. 2013; 45:97–103. [PubMed: 23809879]
3. Anderton SM. Post-translational modifications of self antigens: implications for autoimmunity. Curr Opin Immunol. 2004; 16:753–758. [PubMed: 15511669]
4. Bhat S, Mary S, Banarjee R, Giri AP, Kulkarni MJ. Immune response to chemically modified proteome. Proteomics Clin Appl. 2014; 8:19–34. [PubMed: 24375944]
5. Doyle HA, Mamula MJ. Post-translational protein modifications in antigen recognition and autoimmunity. Trends Immunol. 2001; 22:443–449. [PubMed: 11473834]
6. Valesini G, Gerardi MC, Iannuccelli C, Pacucci VA, Pendolino M, Shoenfeld Y. Citrullination and autoimmunity. Autoimmun Rev. 2015; 14:490–497. [PubMed: 25636595]
7. McInnes IB, Schett G. The pathogenesis of rheumatoid arthritis. N Engl J Med. 2011; 365:2205–2219. [PubMed: 22150039]

8. Bongartz T, Nannini C, Medina-Velasquez YF, Achenbach SJ, Crowson CS, Ryu JH, Vassallo R, Gabriel SE, Matteson EL. Incidence and mortality of interstitial lung disease in rheumatoid arthritis: A population based study. Arthritis Rheum. 2010

9. Brown KK. Rheumatoid lung disease. Proc Am Thorac Soc. 2007; 4:443–448. [PubMed: 17684286]

10. Korkmaz C, Us T, Kasifoglu T, Akgun Y. Anti-cyclic citrullinated peptide (CCP) antibodies in patients with long-standing rheumatoid arthritis and their relationship with extra-articular manifestations. Clin Biochem. 2006; 39:961–965. [PubMed: 16979149]

11. Naz SM, Symmons DP. Mortality in established rheumatoid arthritis. Best Pract Res Clin Rheumatol. 2007; 21:871–883. [PubMed: 17870033]

12. Turesson C, Jacobsson LT. Epidemiology of extra-articular manifestations in rheumatoid arthritis. Scand J Rheumatol. 2004; 33:65–72. [PubMed: 15163106]

13. Young A, Koduri G. Extra-articular manifestations and complications of rheumatoid arthritis. Best Pract Res Clin Rheumatol. 2007; 21:907–927. [PubMed: 17870035]

14. Young A, Koduri G, Batley M, Kulinskaya E, Gough A, Norton S, Dixey J. g. Early Rheumatoid Arthritis Study. Mortality in rheumatoid arthritis. Increased in the early course of disease, in ischaemic heart disease and in pulmonary fibrosis. Rheumatology (Oxford). 2007; 46:350–357. [PubMed: 16908509]

15. Klareskog L, Widhe M, Hermansson M, Ronnelid J. Antibodies to citrullinated proteins in arthritis: pathology and promise. Curr Opin Rheumatol. 2008; 20:300–305. [PubMed: 18388522]

16. del Val del Amo N, Ibanez Bosch R, Fito Manteca C, Gutierrez Polo R, Loza Cortina E. Anti-cyclic citrullinated peptide antibody in rheumatoid arthritis: relation with disease aggressiveness. Clin Exp Rheumatol. 2006; 24:281–286. [PubMed: 16870095]

17. Forslind K, Ahlmen M, Eberhardt K, Hafstrom I, Svensson B. BARFOT Study Group. Prediction of radiological outcome in early rheumatoid arthritis in clinical practice: role of antibodies to citrullinated peptides (anti-CCP). Ann Rheum Dis. 2004; 63:1090–1095. [PubMed: 15308518]

18. Kroot EJ, de Jong BA, van Leeuwen MA, Swinkels H, van den Hoogen FH, van't Hof M, van de Putte LB, van Rijswijk MH, van Venrooij WJ, van Riel PL. The prognostic value of anti-cyclic citrullinated peptide antibody in patients with recent-onset rheumatoid arthritis. Arthritis Rheum. 2000; 43:1831–1835. [PubMed: 10943873]

19. Aggarwal R, Liao K, Nair R, Ringold S, Costenbader KH. Anti-citrullinated peptide antibody assays and their role in the diagnosis of rheumatoid arthritis. Arthritis Rheum. 2009; 61:1472–1483. [PubMed: 19877103]

20. Swart A, Burlingame RW, Gurtler I, Mahler M. Third generation anti-citrullinated peptide antibody assay is a sensitive marker in rheumatoid factor negative rheumatoid arthritis. Clin Chim Acta. 2012; 414:266–272. [PubMed: 23022338]

21. Scally SW, Petersen J, Law SC, Dudek NL, Nel HJ, Loh KL, Wijeyewickrema LC, Eckle SB, van Heemst J, Pike RN, McCluskey J, Toes RE, La Gruta NL, Purcell AW, Reid HH, Thomas R, Rossjohn J. A molecular basis for the association of the HLA-DRB1 locus, citrullination, and rheumatoid arthritis. J Exp Med. 2013; 210:2569–2582. [PubMed: 24190431]

22. van der Helm-van Mil AH, Verpoort KN, Breedveld FC, Huizinga TW, Toes RE, de Vries RR. The HLA-DRB1 shared epitope alleles are primarily a risk factor for anti-cyclic citrullinated peptide antibodies and are not an independent risk factor for development of rheumatoid arthritis. Arthritis Rheum. 2006; 54:1117–1121. [PubMed: 16572446]

23. Viatte S, Plant D, Raychaudhuri S. Genetics and epigenetics of rheumatoid arthritis. Nat Rev Rheumatol. 2013; 9:141–153. [PubMed: 23381558]

24. Klareskog L, Stolt P, Lundberg K, Kallberg H, Bengtsson C, Grunewald J, Ronnelid J, Harris HE, Ulfgren AK, Rantapaa-Dahlqvist S, Eklund A, Padyukov L, Alfredsson L. A new model for an etiology of rheumatoid arthritis: smoking may trigger HLA-DR (shared epitope)-restricted immune reactions to autoantigens modified by citrullination. Arthritis Rheum. 2006; 54:38–46. [PubMed: 16385494]

25. Stolt P, Yahya A, Bengtsson C, Kallberg H, Ronnelid J, Lundberg I, Klareskog L, Alfredsson L. EIRA Study Group. Silica exposure among male current smokers is associated with a high risk of developing ACPA-positive rheumatoid arthritis. Ann Rheum Dis. 2010; 69:1072–1076. [PubMed: 19966090]

26. van der Helm-van Mil AH, Verpoort KN, le Cessie S, Huizinga TW, de Vries RR, Toes RE. The HLA-DRB1 shared epitope alleles differ in the interaction with smoking and predisposition to antibodies to cyclic citrullinated peptide. Arthritis Rheum. 2007; 56:425–432. [PubMed: 17265477]
27. Makrygiannakis D, Hermansson M, Ulfgren AK, Nicholas AP, Zendman AJ, Eklund A, Grunewald J, Skold CM, Klareskog L, Catrina AI. Smoking increases peptidylarginine deiminase 2 enzyme expression in human lungs and increases citrullination in BAL cells. Ann Rheum Dis. 2008; 67:1488–1492. [PubMed: 18413445]
28. Catrina AI, Ytterberg AJ, Reynisdottir G, Malmstrom V, Klareskog L. Lungs, joints and immunity against citrullinated proteins in rheumatoid arthritis. Nat Rev Rheumatol. 2014; 10:645–653. [PubMed: 25072264]
29. Harlow L I, Rosas O, Gochuico BR, Mikuls TR, Dellaripa PF, Oddis CV, Ascherman DP. Identification of citrullinated hsp90 isoforms as novel autoantigens in rheumatoid arthritis-associated interstitial lung disease. Arthritis Rheum. 2013; 65:869–879. [PubMed: 23400887]
30. Harlow L, Gochuico BR, Rosas IO, Doyle TJ, Osorio JC, Travers TS, Camacho CC, Oddis CV, Ascherman DP. Anti-citrullinated heat shock protein 90 antibodies identified in bronchoalveolar lavage fluid are a marker of lung-specific immune responses. Clin Immunol. 2014; 155:60–70. [PubMed: 25150019]
31. Tarcsa E, Marekov LN, Mei G, Melino G, Lee SC, Steinert PM. Protein unfolding by peptidylarginine deiminase. Substrate specificity and structural relationships of the natural substrates trichohyalin and filaggrin. J Biol Chem. 1996; 271:30709–30716. [PubMed: 8940048]
32. Pritzker LB, Joshi S, Gowan JJ, Harauz G, Moscarello MA. Deimination of myelin basic protein. 1. Effect of deimination of arginyl residues of myelin basic protein on its structure and susceptibility to digestion by cathepsin D. Biochemistry. 2000; 39:5374–5381. [PubMed: 10820008]
33. Nijenhuis S, Zendman AJ, Vossenaar ER, Pruijn GJ, vanVenrooij WJ. Autoantibodies to citrullinated proteins in rheumatoid arthritis: clinical performance and biochemical aspects of an RA-specific marker. Clin Chim Acta. 2004; 350:17–34. [PubMed: 15530456]
34. Terao C, Ohmura K, Katayama M, Takahashi M, Kokubo M, Diop G, Toda Y, Yamamoto N, Shinkura R, Shimizu M, Gut I, Heath S, Melchers I, Manabe T, Lathrop M, Mimori T, Yamada R, Matsuda F. G. Human Disease Genomics Working, C. Rheumatoid Arthritis, C. Genetic Study. Myelin basic protein as a novel genetic risk factor in rheumatoid arthritis--a genome-wide study combined with immunological analyses. PLoS One. 2011; 6:e20457. [PubMed: 21673997]
35. Arnett FC, Edworthy SM, Bloch DA, McShane DJ, Fries JF, Cooper NS, Healey LA, Kaplan SR, Liang MH, Luthra HS, et al. The American Rheumatism Association 1987 revised criteria for the classification of rheumatoid arthritis. Arthritis Rheum. 1988; 31:315–324. [PubMed: 3358796]
36. Mikuls TR, Kazi S, Cipher D, Hooker R, Kerr GS, Richards JS, Cannon GW. The association of race and ethnicity with disease expression in male US veterans with rheumatoid arthritis. J Rheumatol. 2007; 34:1480–1484. [PubMed: 17552044]
37. Gochuico BR, Avila NA, Chow CK, Novero LJ, Wu HP, Ren P, MacDonald SD, Travis WD, Stylianou MP, Rosas IO. Progressive preclinical interstitial lung disease in rheumatoid arthritis. Arch Intern Med. 2008; 168:159–166. [PubMed: 18227362]
38. Lee CC, Lin TW, Ko TP, Wang AH. The hexameric structures of human heat shock protein 90. PLoS One. 2011; 6:e19961. [PubMed: 21647436]
39. Myers EW, Miller W. Optimal alignments in linear space. Comput Appl Biosci. 1988; 4:11–17. [PubMed: 3382986]
40. Schrödinger, LLC. The PyMOL Molecular Graphics System, Version 1.7.4.0.
41. Case, DA.; Berryman, JT.; Betz, RM.; Cerutti, DS.; Cheatham, TE., III; Darden, TA.; Duke, RE.; Giese, TJ.; Gohlke, H.; Goetz, AW.; Homeyer, N.; Izadi, S.; Janowski, P.; Kaus, J.; Kovalenko, A.; Lee, TS.; LeGrand, S.; Li, P.; Luchko, T.; Luo, R.; Madej, B.; Merz, KM.; Monard, G.; Needham, P.; Nguyen, H.; Nguyen, HT.; Omelyan, I.; Onufriev, A.; Roe, DR.; Roitberg, A.; Salomon-Ferrer, R.; Simmerling, CL.; Smith, W.; Swails, J.; Walker, RC.; Wang, J.; Wolf, RM.; Wu, X.; York, DM.; Kollman, PA. AMBER 2015. University of California; San Francisco: 2015.

42. Salomon-Ferrer R, Gotz AW, Poole D, Le Grand S, Walker RC. Routine Microsecond Molecular Dynamics Simulations with AMBER on GPUs. 2. Explicit Solvent Particle Mesh Ewald. J Chem Theory Comput. 2013; 9:3878–3888. [PubMed: 26592383]
43. Maier JA, Martinez C, Kasavajhala K, Wickstrom L, Hauser KE, Simmerling C. ff14SB: Improving the Accuracy of Protein Side Chain and Backbone Parameters from ff99SB. J Chem Theory Comput. 2015; 11:3696–3713. [PubMed: 26574453]
44. Petrov D, Margreitter C, Grandits M, Oostenbrink C, Zagrovic B. A systematic framework for molecular dynamics simulations of protein post-translational modifications. PLoS Comput Biol. 2013; 9:e1003154. [PubMed: 23874192]
45. Jorgensen WL. Quantum and statistical mechanical studies of liquids. 10. Transferable intermolecular potential functions for water, alcohols, and ethers. Application to liquid water. J Am Chem Soc. 1981; 103:335–340.
46. Darden T, York D, Pedersen L. Particle mesh Ewald: An N·log(N) method for Ewald sums in large systems. The Journal of Chemical Physics. 1993; 98:10089–10092.
47. Feenstra KA, Hess B, Berendsen HJC. Improving efficiency of large time-scale molecular dynamics simulations of hydrogen-rich systems. J Comput Chem. 1999; 20:786–798.
48. Miyamoto S, Kollman PA. Settle: An analytical version of the SHAKE and RATTLE algorithm for rigid water models. J Comput Chem. 1992; 13:952–962.
49. Ryckaert JP, Ciccotti G, Berendsen HJC. Numerical integration of the cartesian equations of motion of a system with constraints: molecular dynamics of n-alkanes. Journal of Computational Physics. 1977; 23:327–341.
50. Sinko W, Miao Y, de Oliveira CA, McCammon JA. Population based reweighting of scaled molecular dynamics. J Phys Chem B. 2013; 117:12759–12768. [PubMed: 23721224]
51. Humphrey W, Dalke A, Schulten K. VMD: visual molecular dynamics. J Mol Graph. 1996; 14:33–38. 27–38. [PubMed: 8744570]
52. Roe DR, Cheatham TE 3rd. PTRAJ and CPPTRAJ: Software for Processing and Analysis of Molecular Dynamics Trajectory Data. J Chem Theory Comput. 2013; 9:3084–3095. [PubMed: 26583988]
53. Chirivi RGS, van Rosmalen JWG, Jenniskens GJ, Pruijn GJ, Raats JMH. Citrullination: A Target for Disease Intervention in Multiple Sclerosis and other Inflammatory Diseases? J Clin Cell Immunol. 2013; 4:146.
54. Brinkmann V, Reichard U, Goosmann C, Fauler B, Uhlemann Y, Weiss DS, Weinrauch Y, Zychlinsky A. Neutrophil extracellular traps kill bacteria. Science. 2004; 303:1532–1535. [PubMed: 15001782]
55. Khandpur R, Carmona-Rivera C, Vivekanandan-Giri A, Gizinski A, Yalavarthi S, Knight JS, Friday S, Li S, Patel RM, Subramanian V, Thompson P, Chen P, Fox DA, Pennathur S, Kaplan MJ. NETs are a source of citrullinated autoantigens and stimulate inflammatory responses in rheumatoid arthritis. Sci Transl Med. 2013; 5:178ra140.
56. Shoda H, Fujio K, Shibuya M, Okamura T, Sumitomo S, Okamoto A, Sawada T, Yamamoto K. Detection of autoantibodies to citrullinated BiP in rheumatoid arthritis patients and pro-inflammatory role of citrullinated BiP in collagen-induced arthritis. Arthritis Res Ther. 2011; 13:R191. [PubMed: 22108001]
57. Wisniewska M, Karlberg T, Lehtio L, Johansson I, Kotenyova T, Moche M, Schuler H. Crystal structures of the ATPase domains of four human Hsp70 isoforms: HSPA1L/Hsp70-hom, HSPA2/Hsp70-2, HSPA6/Hsp70B′, and HSPA5/BiP/GRP78. PLoS One. 2010; 5:e8625. [PubMed: 20072699]

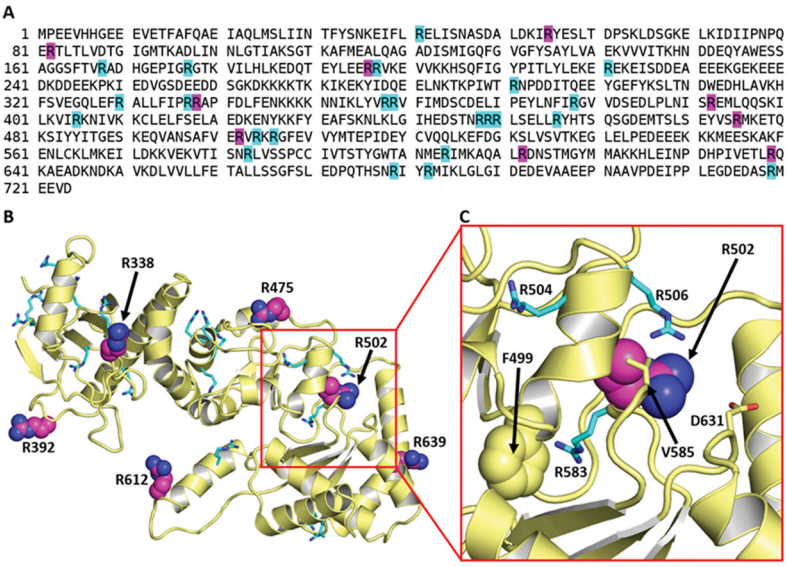

Figure 1. A cryptic epitope is buried in native HSP90β

(A) Sequence of human HSP90β immunoprecipitated by RA-ILD serum demonstrates 9 arginines targeted by *in vitro* citrullination (magenta) of whole cell extract as well as the remaining unmodified arginines (cyan) (29). **(B)** Homology model depicts the middle domain structure of HSP90β corresponding to residues 303–706. Six of the nine previously identified citrullination sites are shown as magenta spheres; other arginines are shown as cyan sticks. **(C)** Magnified view of boxed portion of (B) showing the region surrounding peptide 7/R502. While residues V585 and D631 are shown as sticks, the buried residue F499 is represented by spheres.

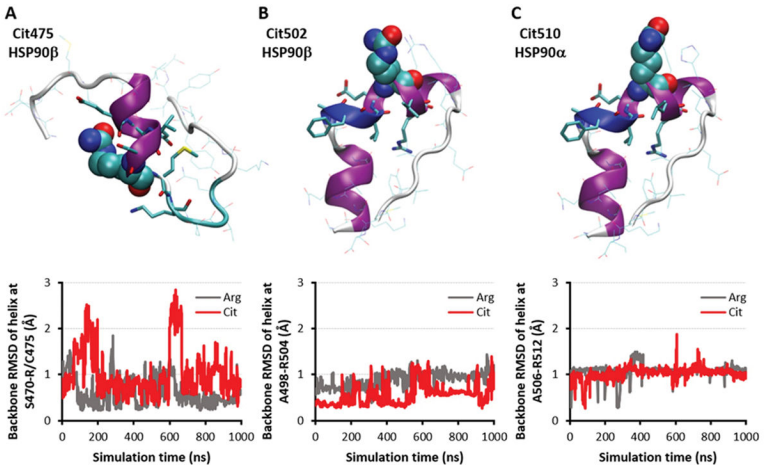

Figure 2. Citrulline-specific antigenic peptides possess stable native-like secondary structure both with and without citrullination

Starting peptide conformations (top) and backbone RMSD plots of indicated helical regions over 1-μs MD simulations (bottom) for **(A)** HSP90β peptide 6 (site R475), **(B)** HSP90β peptide 7 (site R502), and **(C)** HSP90α peptide 10 (site R510). Modified arginines are shown as spheres, while nearby residues are shown as sticks.

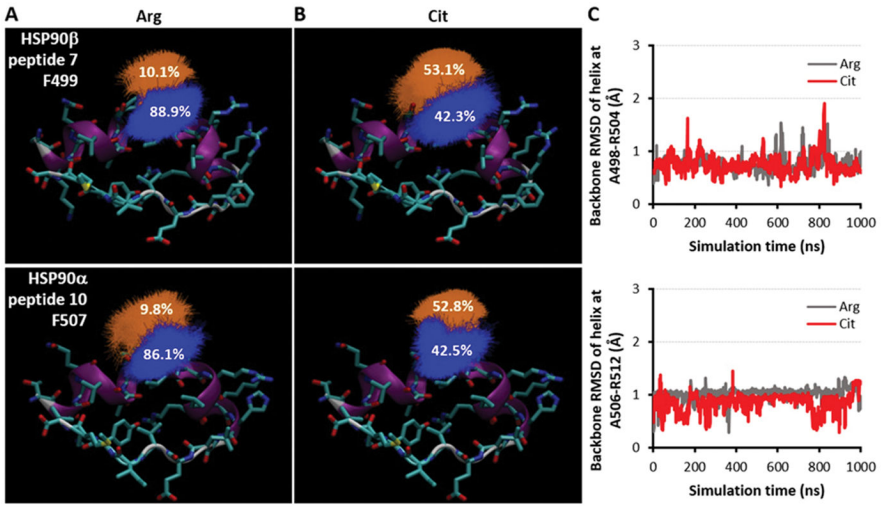

Figure 3. Peptide and side chain stability of cryptic epitope in HSP90β/α

(A) Clustering of sampled side chain orientations for F499 in HSP90β peptide 7 (top) and F507 in HSP90α peptide 10 (bottom) based on MD simulations of the uncitrullinated peptides. **(B)** Similar clustering analysis for MD simulations of the citrullinated peptide. **(C)** Backbone RMSD plots of helical regions over 1-μs MD simulations of F499A peptide 7 (top) and F507A peptide 10 (bottom).

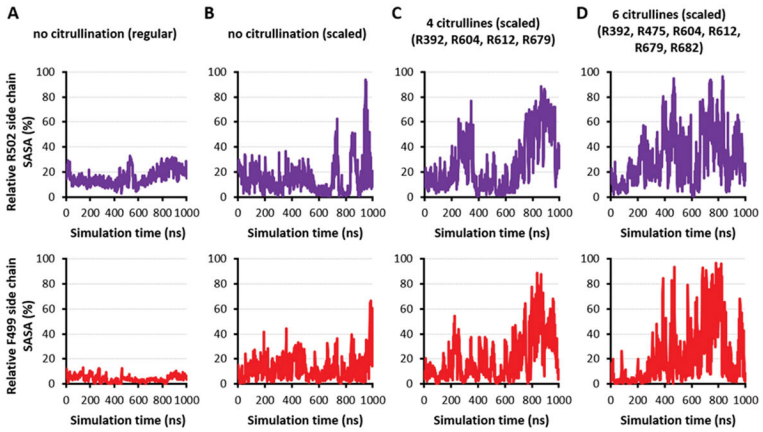

Figure 4. Increasing number of citrullines unfolds HSP90

Plots of relative side chain solvent-accessible surface area (SASA) measurements for R502 (top row) and F499 (bottom row) over 1-μs *conventional* MD simulations for the middle domain of HSP90β (comprising residues 286–691) with no citrullines **(A)** versus 1-μs *scaled* MD simulations of the same domain with **(B)** no citrullines, **(C)** four citrulline modifications at R392, R604, R612, and R679, and **(D)** six citrulline modifications that include residues designated in (C) as well as R475 and R682.

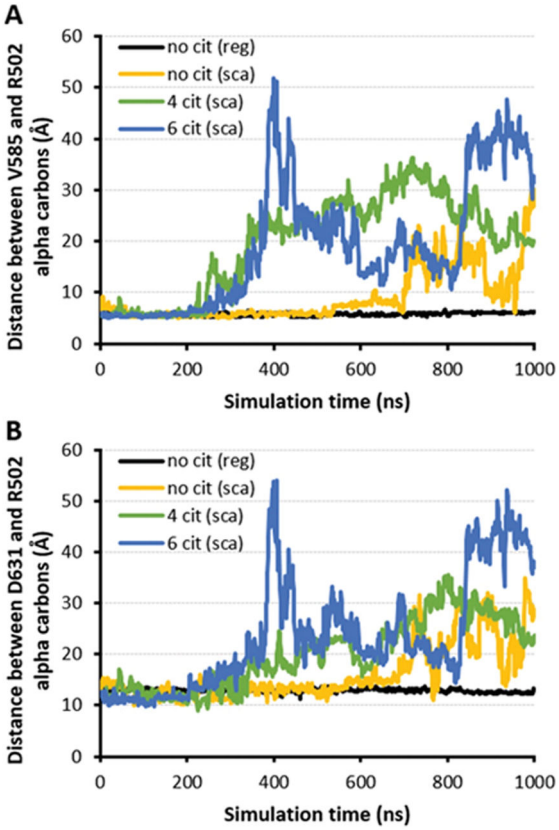

Figure 5. Core of HSP90β opens up between peptide 7 and surrounding domains following multiple arginine-citrulline conversions

Designated plots depict the distance between alpha-carbons of R502 and **(A)** V585 or **(B)** D631 over 1 μs conventional (black curve) or scaled MD simulations (yellow, green, and blue curves for 0, 4, and 6 citrullines, respectively) of HSP90β.

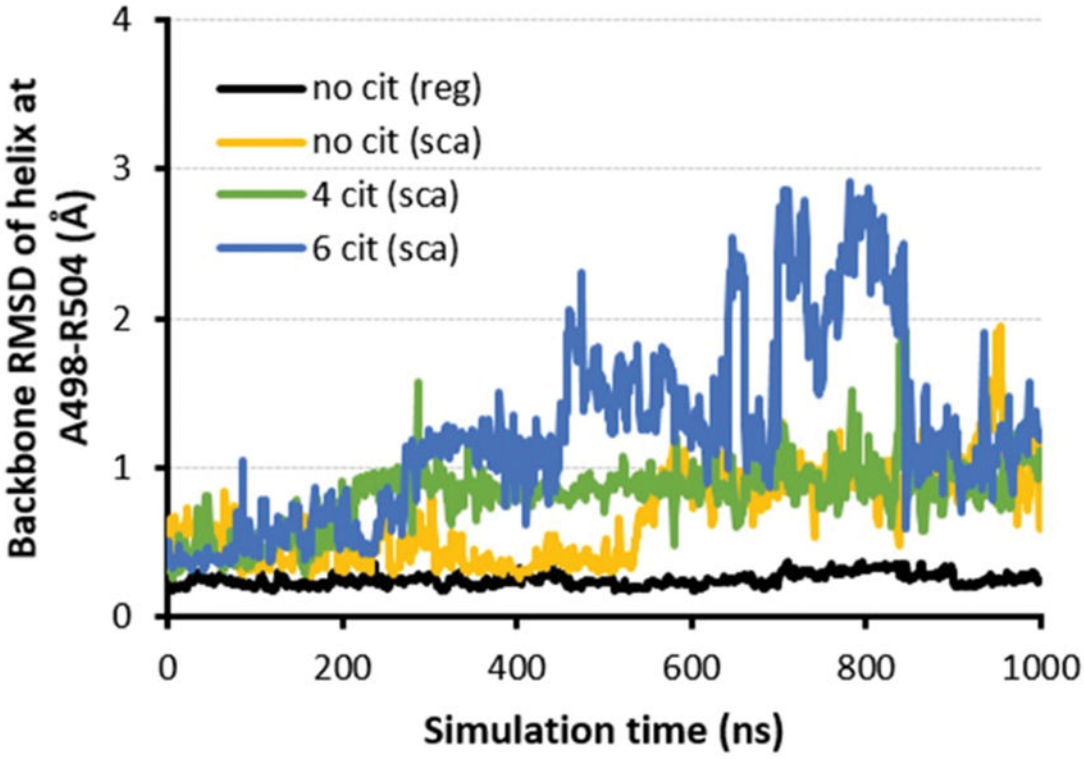

Figure 6. Helical domain of cryptic peptide remains stable (RMSD ~ 1Å) upon citrullination-induced unfolding of HSP90β

Backbone RMSD plots demonstrate relative stability of helical region around citrullination site R502 over 1 μs conventional (black curve) or scaled MD simulations (yellow, green, and blue curves for 0, 4, and 6 citrullines, respectively) of variably citrullinated HSP90β.

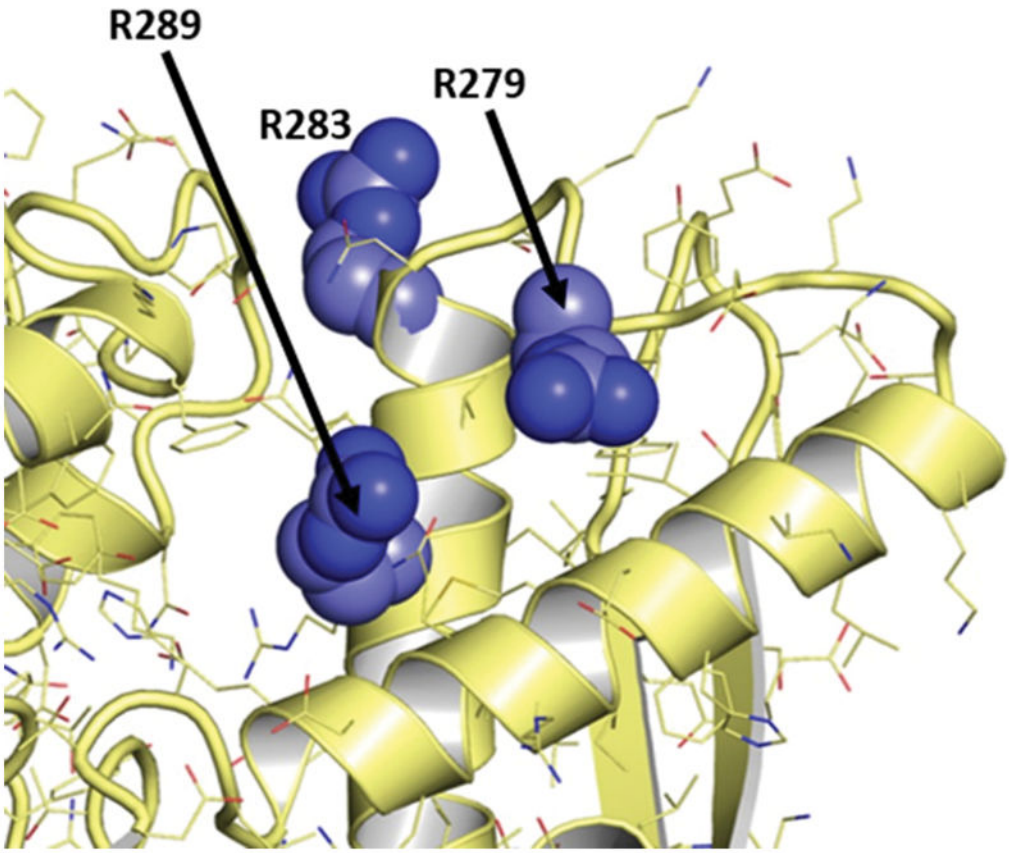

Figure 7. RA patient sera show strong antibody recognition of citrullinated R289 that is buried in structure of BiP

Nearby sites at R279 and R283 are solvent-exposed, but they are not targeted by autoantibodies derived from RA patient sera. Structure taken from PDB ID 3IUC (57).

Table I

HSP90-derived 25-mer peptides containing citrullination sites identified by mass spectrometric analysis of citrullinated proteins immunoprecipitated by RA-ILD patient sera (29).

1-R) LISNASDALDKI-R-YESLTDPSKLDS	55[1]	1-C) LISNASDALDKI-C-YESLTDPSKLDS
2-R) ELKIDIIPNPQE-R-TLTLVDTGIGMT	82	2-C) ELKIDIIPNPQE-C-TLTLVDTGIGMT
3-R) HLKEDQTEYLEE-R-RVKEVVKKHSQF	196	3-C) HLKEDQTEYLEE-C-RVKEVVKKHSQF
4-R) QLEFRALLFIPR-R-APFDLFENKKKK	338	4-C) QLEFRALLFIPR-C-APFDLFENKKKK
5-R) VVDSEDLPLNIS-R-EMLQQSKILKVI	392	5-C) VVDSEDLPLNIS-C-EMLQQSKILKVI
6-R) GDEMTSLSEYVS-R-MKETQKSIYYIT	475	6-C) GDEMTSLSEYVS-C-MKETQKSIYYIT
7-R) SKEQVANSAFVE-R-VRKRGFEVVYMT	502	7-C) SKEQVANSAFVE-C-VRKRGFEVVYMT
8-R) ANMERIMKAQAL-R-DNSTMGYMMAKK	612	8-C) ANMERIMKAQAL-C-DNSTMGYMMAKK
9-R) EINPDHPIVETL-R-QKAEADKNDKAV	639	9-C) EINPDHPIVETL-C-QKAEADKNDKAV
10-R) TKDQVANSAFVE-R-LRKHGLEVIYMI	510[2]	10-C) TKDQVANSAFVE-C-LRKHGLEVIYMI

[1]Position of the citrullination site in the full protein sequence. Wild-type (uncitrullinated) and citrullinated peptide sequences (with citrullination site between dashes) are shown on the left and right, respectively.

[2]Peptides 1-R/1-C to 9-R/9-C were derived from HSP90β; peptides 10-R/10-C were derived from HSP90α.

Table II

Citrullination results from mass spectrometry analysis of HSP90β incubated with high concentration (5 units/mL) of PAD.[1]

Incubation Time	Citrullinated residues identified																		
30 min	82		177					**392**		475		504			**604**	**612**	639	**679**	682
60 min	82		177					**392**	449	475			506		**604**	**612**		**679**	682
120. min	82	168	177					**392**			**502**				**604**	**612**		**679**	682
360 min	82	168	177					**392**					506	583	**604**	**612**		**679**	
overnight	82	168	177	196	197	291	337	**392**	449	475	**502**	504	506		**604**	**612**		**679**	682

[1] representative of 3 independent experiments

Table III

Citrullination results from mass spectrometry analysis of HSP90β incubated with low concentrations (0.5 units/mL) of PAD.[1]

Incubation Time	Citrullinated residues identified														
30 min	82		177		378	392		475	504	604	612			682	
60 min			177	196						604	612				
120. min	82	168			378	392		475		604	612		679		
360 min	82					392			504	604	612		679	682	
overnight	82	168	177	291		392	448	456	**502**	604	612	639	679	682	

[1] representative of two independent experiments, with some variability based on MS coverage

J Immunol. Author manuscript; available in PMC 2017 September 01.

Table IV

ELISA results comparing serum recognition of wild-type (uncitrullinated) vs. citrullinated versions of HSP90-derived peptides.

	1C:1R	2C:2R	3C:3R	4C:4R	5C:5R	6C:6R	7C:7R	8C:8R	9C:9R	10C:10R
DA005	−:−	−:−	−:−	−:−	−:−	+++:-	+++:-	−:−	−:−	+++:-
DA023	−:−	−:−	−:−	−:−	−:−	+++:-	+++:+	−:−	−:−	+/−:−
DA217	−:−	−:−	−:−	−:−	−:−	+++:-	+/−:−	+:+	−:−	−:−
DA233	−:−	−:−	−:−	−:−	−:−	−:−	−:−	−:−	−:−	−:−
DA380	−:−	−:−	++:+	−:−	−:−	−:−	−:−	−:−	−:−	−:−
DA459	-:+	−:−	+:-	+++:-	+++:-	++:+/-	+++:+	+/−:+/−	−:−	++:+/-
DA485	−:−	−:−	−:−	−:−	−:−	++:-	+++:+	+/−:−	+++:+++	++:-
DC058	−:−	−:−	−:−	−:−	−:−	−:−	−:−	−:−	−:−	−:−
DV049	−:−	−:−	++:-	+/−:−	+:-	−:−	−:−	+:-	−:−	−:−
DV057	−:−	−:−	−:−	−:−	−:−	+:-	++:-	+:-	−:−	+/−:−
DV075	−:−	−:−	−:−	−:−	−:−	+++:-	+++: +	+/−:−	+:-	++:-
DV092	−:−	−:−	−:−	−:−	−:−	−:−	++:-	−:−	−:−	−:−
DV097	−:−	−:−	+:-	−:−	+++:-	+++:+/-	+++:-	−:−	+/−:−	+/−:−
DV116	−:−	−:−	+++:-	++:-	+:+	+++:-	+++:-	−:−	−:−	+++:+
OM014	−:−	−:−	−:−	−:−	−:−	−:−	−:−	−:−	−:−	−:−

	1C:1R	2C:2R	3C:3R	4C:4R	5C:5R	6C:6R	7C:7R	8C:8R	9C:9R	10C:10R
OM053	−:+/−	−:−	+:−	−:−	+/−:−	+:+:+/-	+:+:+:+	+/−:−	−:−	+:+:+:-
OM090	−:+/−	−:−	+:−	+:+/-	+:+:+:+/-	+:+:+/-	+:+:+	+:+:−	+/-:+	+:+/-
SL088	−:−	+:−	−:−	−:−	−:−	+:+:+:-	+:+:+:+/-	+:+/-	−:−	+:-
131a	−:−	−:−	−:−	−:−	−:−	−:−	−:−	−:−	−:−	−:−
16a	−:−	−:−	−:−	−:−	+:+:+:+	+/-:+	−:−	−:−	−:−	+/−:−
1a	−:−	−:−	−:−	−:−	−:−	−:−	−:−	−:−	−:−	−:−
82a	−:−	−:−	−:−	−:−	−:−	+:-	+:-	−:−	−:−	−:−
83a	−:−	+:−	−:−	−:−	−:−	−:−	−:−	−:−	−:−	−:−
126a	−:−	−:−	−:−	−:−	−:−	−:−	−:−	−:−	−:−	−:−
138a	−:−	−:−	−:−	−:−	+:+:+:+	−:−	−:−	−:−	−:−	−:−
41a	−:−	−:−	−:−	−:−	−:−	−:−	−:−	−:−	−:−	−:−
144	−:−	−:−	−:−	−:−	−:−	−:−	−:−	−:−	−:−	−:−
162	−:−	−:−	+/−:−	−:−	+:+	−:−	−:−	−:−	−:−	−:−
99b	−:−	−:−	−:−	−:−	−:−	−:−	−:−	−:−	−:−	−:−
170	−:−	−:−	−:−	−:−	−:−	−:−	−:−	−:−	−:−	−:−
178	−:−	−:−	−:−	−:−	−:−	−:−	−:−	−:−	−:−	−:−
111	−:−	−:−	−:−	−:−	−:−	−:−	−:−	−:−	−:−	−:−
98	−:−	−:−	−:−	−:−	−:−	−:−	−:−	−:−	−:−	−:−
179	−:−	−:−	−:−	−:−	−:−	−:−	−:−	−:−	−:−	−:−
191	−:−	−:−	−:−	−:−	−:−	+:+:+:+	+:+:+	−:−	−:−	+/−:−
60a	−:−	−:−	−:−	−:−	−:−	−:−	−:−	−:−	−:−	−:−

	1C:1R	2C:2R	3C:3R	4C:4R	5C:5R	6C:6R	7C:7R	8C:8R	9C:9R	10C:10R
121a	−:−	−:−	+++	+/−:−	−:−	+++	+/−:−	−:−	−:−	−:−
122a	−:−	−:−	−:−	−:−	−:−	+++	+/−:−	+++	−:−	−:−

RA-ILD

RA-subILD

RA-no ILD

Peptides: uncitrullinated: 1–10; citrullinated: 1C-10C

− = OD 0–0.1

+/− = OD 0.1–0.2

+ = OD 0.2–0.5

++ = OD 0.5–1.0

+++ = OD > 1.0

Table V

ELISA results comparing binding of uncitrullinated vs. citrullinated versions of peptides 7 and 10 (derived from HSP90β and HSP90α, respectively), either with or without an F→A mutation at residue 499 (peptide 7) or 507 (peptide 10).

	Peptide 7 (HSP90β)				Peptide 10 (HSP90α)			
	WT R502	**WT Cit502**	**F499A/F508L R502**	**F499A/F508L Cit502**	**WT R510**	**WT Cit510**	**F507A R510**	**F507A Cit510**
RA-ILD								
DV097	+/−	+++	−	−	−	+/−	−	−
DA023	−	+++	−	+/−	−	+/−	−	−
OM053	+/−	+++	−	+/−	−	+++	−	−

− = OD 0–0.1

+/− = OD 0.1–0.2

+ = OD 0.2–0.5

++ = OD 0.5–1.0

+++ = OD > 1.0

Table VI

Antibody recognition of variably citrullinated HSP90β[1,2]

	citHSP90β-30 min	citHSP90β-120 min	citHSP90β-overnight
15	0.69	0.70	1
34	0.59	0.86	1
144	<0.01	0.54	1
162	0.79	1.06	1
13-B	0.68	1.04	1
18-B	0.33	0.71	1
25-B	0.24	0.29	1
PT-1	0.25	0.51	1
131	0.39	0.67	1
59	0.8	1.04	1
DA485	0.24	0.55	1
DV057	0.28	0.45	1
DV092	1.03	1.50	1

[1] values equal ratio of OD_{450} (citHSP90β - HSP90β)-time "x" to OD_{450} (citHSP90β - HSP90β)-time overnight, where x equals duration of PAD-mediated deimination; the absolute OD_{450} values for (citHSP90β - HSP90β)-overnight ranged from 0.2–1.0

[2] control polyclonal anti-HSP90 antibody binding confirmed equal amounts of substrate HSP90β preparations bound to ELISA plates

RA-no ILD

RA-subILD

RA-ILD